Research Square

Preprints are preliminary reports that have not undergone peer review.
They should not be considered conclusive, used to inform clinical practice,
or referenced by the media as validated information.

Granzyme A-expressing Terminal Effector T Cells Dedifferentiate into Long-lived Memory T Cells

Nu Zhang

ZhangN3@uthscsa.edu

University of Texas Health Science Center at San Antonio https://orcid.org/0000-0001-9695-210X

Chaoyu Ma

The University of Texas Health Science Center at San Antonio

Wei Liao

Department of Dermatology, Hunan Children's Hospital

Saranya Srinivasan

University of Texas Health San Antonio

Chenhui he

University of Texas Health San Antonio

Kenneth Fan

University of Texas Health San Antonio

Tyng-An Zhou

University of Texas Health San Antonio

Courtney Segura-Cepero

University of Texas Health San Antonio

Heetanshi Jain

University of Texas Health San Antonio

Sahana Jayakumar

University of Texas Health San Antonio

Weiguo Cui

Northwestern University Feinberg School of Medicine https://orcid.org/0000-0003-1562-9218

Yu Luan

University of Texas Health San Antonio

Article

Keywords:

Posted Date: June 26th, 2026

DOI: https://doi.org/10.21203/rs.3.rs-10107441/v1

License: This work is licensed under a Creative Commons Attribution 4.0 International License.
Read Full License

Additional Declarations: There is **NO** Competing Interest.

Abstract

Memory T cells are critical for vaccines and T-cell-based therapies. However, the differentiation path of memory T cells is not completely understood. Early bulk cell population-based studies support a linear model, in which effector T cells lose the effector program and dedifferentiate into memory T cells. Recent research supports a bifurcation model, where T cells choose one of the two paths, either the effector or the memory path, at an early stage of T cell responses. Terminal effector T cells lose the capacity to become memory T cells. Here, we first demonstrate that the expression of granzyme A is largely distinct from that of granzyme B and marks terminal cytotoxic effector $CD8^+$ T cells with reduced polyfunctionality. Using a granzyme A-fate mapping mouse line and an acute viral infection model, we discovered that early memory T cells are largely derived from cells lacking a history of granzyme A expression, supporting the bifurcation model. Progressively, granzyme A-expressing terminal effector T cells dedifferentiate into functional long-term memory T cells. At the late memory phase, memory T cells are a mixed population composed of cells with different differentiation paths (i.e., the linear and the bifurcated paths) that coordinate to provide balanced immune protection.

Introduction

Memory T cells (T_{MEM}) are one of the key components of immunological memory, serving as the cellular basis for various T cell-based vaccines and immunotherapies[1]. The differentiation paths of T_{MEM} have been intensively investigated. Two models, namely the linear differentiation model and the bifurcation model, have been proposed. In the linear model, all primed T cells differentiate into effector T cells. A selected subset of effector T cells can further differentiate into T_{MEM} via a dedifferentiation process (i.e., effector T cells lose the expression of effector molecules to become T_{MEM})[2–6]. In the bifurcation model, after initial priming and an early expansion phase, two subsets of T cells emerge. One will continue to acquire effector functions, including cytotoxicity. This population of effector T cells will undergo contraction after antigen clearance or become long-lived effector T cells[7]. The other subset, so-called memory precursors, will preferentially become T_{MEM} cells, including central memory T cells (T_{CM})[8–15]. It is highly possible that there are multiple divergent points contributing to the bifurcating process, including naïve T cell heterogeneity[16], the first cell division[9, 17], and a few cell cycles after T cell priming[12, 14]. Since the recent evidence overwhelmingly supports the bifurcation model[18], it is generally accepted that a subset of early effector T cells maintains high Tcf-1 (T cell factor-1) expression[13], receives less IL-2 and inflammatory signaling, has undergone less/slower cell cycles[12], and preferentially differentiates into long-term T_{MEM}, especially the T_{CM} population. Further, the memory precursors exhibit enhanced pyrimidine synthesis[15] and are resistant to DNA damage[11]. Importantly, these memory precursor cells lack cytotoxic capacity even at the peak of responses[8].

However, previous research is often performed using bulk T cell subsets or a snapshot of single-cell differentiation status at given stages during an immune response. Long-term tracing of terminal effector

T cells in vivo is largely lacking. Whether terminal effector T cells can make a significant contribution to the long-term memory pool remains unresolved. Here, we generate a genetic fate-mapping strain of mice, in which all granzyme A-expressing effector $CD8^+$ T cells are permanently labelled. We provide evidence that granzyme A expression marks terminal cytotoxic effector T cells with diminished capacity for cytokine production. Using the *Gzma*-fate mapping (*Gzma*-FM) mice, we found that the majority of T_{CM} did not experience a $Gzma^+$ stage, especially at the early memory phase, consistent with the bifurcation model. However, T_{CM} that experienced a $Gzma^+$ phase gradually accumulated over time to a sizable proportion. These dedifferentiated T_{CM} carried a similar level of Tcf-1 expression, exhibited subtle transcriptional changes, and elicited comparable recall responses. Thus, both linear and bifurcation models are operational following acute viral infection. The bifurcation model is the major player at the early stage of memory differentiation, whereas the linear model progressively contributes to the long-term memory T cell pool.

Results

Distinct expression patterns of granzyme A and granzyme B in $CD8^+$ T cells. We first examined the expression of granzyme A and granzyme B during $CD8^+$ T cell activation. Purified naïve $CD8^+$ T cells were activated by aCD3/28 and cultured in IL-2/IL-15 (**Fig. 1A**). As shown in **Fig. 1B**, *Gzmb* was rapidly induced upon T cell activation. In contrast, we did not detect any upregulation of *Gzma* within the same culture period. To determine the expression of *Gzma* vs *Gzmb* in memory $CD8^+$ T cells, we employed an experimental design illustrated in **Fig. 1C**. Briefly, naïve P14 TCR transgenic $CD8^+$ T cells were adoptively transferred into C57BL/6 (B6) recipients, followed by LCMV (Lymphocytic choriomeningitis virus) Armstrong infection. P14 T cells recognize an immunodominant epitope derived from LCMV (i.e., $H\text{-}2D^b\text{-}GP_{33\text{-}41}$). Thirty days post-LCMV infection, memory P14 T cells were subjected to two different recall stimuli *in vivo*: antigen-specific stimulation via cognate peptide and bystander inflammation via systemic LM (*Listeria monocytogenes*) infection. To directly assess the production of effector molecules without *in vitro* culture, BFA (Brefeldin A) was injected *in vivo*. As expected, both bystander inflammation and TCR stimulation induced robust memory T cell activation as demonstrated by increased CD69 expression (**Fig. 1D**), cell size (**Fig. 1E**), and IFN-g production (**Fig. 1F**). Interestingly, we only detected TNF-a production in TCR, but not bystander-stimulated memory T cells (**Fig. 1G**). Similar to other activation markers, the expression of granzyme B was induced by both bystander and TCR stimulation (**Fig. 1H**). In stark contrast, the expression of granzyme A was not affected by bystander inflammation and was significantly reduced upon TCR stimulation (**Fig. 1I**). Thus, during the activation of both naïve and memory $CD8^+$ T cells, the expression patterns of granzyme A and granzyme B are distinct.

Generation of a *Gzma*-fate mapping (*Gzma*-FM) mouse model. We are curious about the unique and dynamic expression pattern of granzyme A in $CD8^+$ T cells. We generated a *Gzma*-Cre mouse strain by knocking in a cDNA cassette containing Cre recombinase into the endogenous *Gzma* locus. We further crossed *Gzma*-Cre mice with the *Rosa26*-LSL-tdTomato Cre reporter line to generate *Gzma*-fate mapping

(*Gzma*-FM) mice (**Fig. S1A**). Presumably due to the low skipping efficiency of P2A and T2A peptides at this locus[19], *Gzma*-Cre allele is a knockout allele for *Gzma* (**Fig. S1B** to **S1D**). We used *Gzma*-Cre/+ heterozygous mice for the following experiments to fate map *Gzma*$^+$ and ex-*Gzma*$^+$ cells.

In naïve *Gzma*-FM mice (*Gzma*-Cre/+; *Rosa26*-LSL-tdTomato), we detected low levels of tdTomato signal during the double negative to double positive transition of thymocyte development, which is consistent with published results that low levels of *Gzma* expression can be detected in the thymus (**Fig. S1E**)[20]. In the periphery, around 10% of both naive CD4$^+$ and CD8$^+$ T cells carried tdTomato expression, comparable to mature single positive thymocytes. CD44^{hi} CD8$^+$, but not CD44$^+$CD4$^+$ T cells, contained a significantly elevated proportion of tdTomato$^+$ cells. As expected, most NK cells were tdTomato$^+$ (**Fig. S1F**). In the intraepithelial lymphocyte compartment of the small intestine (SI-IEL), innate-like T cells (TCRgd$^+$ and CD8aa$^+$TCR-b$^+$) were mostly tdTomato$^+$, whereas conventional TCR-b$^+$ T cells, both tdTomato$^+$ and tdTomato$^-$ cells, were present (**Fig. S1G**). Together, we established a mouse line to fate map *Gzma* expression. Thereafter, we will term tdTomato$^+$ cells in *Gzma*-FM mice as *Gzma*-FM$^+$ cells.

***Gzma*-FM faithfully marks Gzma$^+$ and ex-Gzma$^+$ CD8$^+$ effector and memory T cells**. To track antigen-specific effector and memory T cell differentiation, we backcrossed *Gzma*-FM mice onto B6 background for twelve generations and generated congenically marked *Gzma*-FM-P14 TCR transgenic mice. As shown in **Fig. 2A**, tdTomato$^-$ naïve *Gzma*-FM P14 T cells were FACS-sorted and adoptively transferred into B6 recipients and followed by LCMV infection (input P14 purity shown in **Fig. 2B**). Granzyme A was rarely detectable in early effector CD8$^+$ T cells (day 5.5) and reached the peak level around day 7-8 (**Fig. 2C**), confirming that *Gzma* expression tracks effector CD8$^+$ T cell differentiation, but not T cell activation. Consistent with granzyme A expression, *Gzma*-FM signal was low at day 5 post-infection in the spleen (**Fig. 2D** and **2E**). From the peak of P14 T cell response (day 7-8) to memory phase (>day 30-60), *Gzma*-FM signal was stabilized around 20-30% of P14 T cells in the spleen (**Fig. 2D** to **2F**). After the peak of the response, lymph node (LN) P14 T cells carried fewer *Gzma*-FM$^+$ cells (**Fig. 2E** and **2F**). Among all non-lymphoid tissues that we have examined, the small intestines harbor significantly increased *Gzma*-FM$^+$ cells (**Fig. 2F**), consistent with the notion that intestinal mucosal tissue resident memory T cells (T_{RM}) possess enhanced cytotoxicity. When comparing *Gzma*-FM$^+$ vs *Gzma*-FM$^-$ P14 T cells, the expression of granzyme A was largely restricted to the *Gzma*-FM$^+$ subset in both spleen and small intestine, reassuring that *Gzma*-FM faithfully labels *Gzma*-expressing cells (**Fig. 2G** to **2I**). Importantly, the frequency and distribution of *Gzma*-FM$^+$ cells could be validated in a polyclonal setting in the absence of P14 TCR transgene (**Fig. S2C**).

To provide an additional control, we generated *Gzmb*-FM mice using *Gzmb*-Cre[5] and *Rosa26*-LSL-YFP Cre reporter mice. As illustrated in **Fig. S3A**, YFP$^-$ naïve P14 T cells were FACS-sorted and adoptively transferred into B6 recipients, followed by LCMV infection. Consistent with the findings that *Gzmb* is rapidly induced upon T cell activation (**Fig. 1B**), *Gzmb*-FM labeled more than 90% of donor P14 T cells

across multiple tissues (**Fig. S3B**). Together, we conclude that *Gzma*-FM, but not *Gzmb*-FM, selectively tracks a subset of effector and memory CD8$^+$ T cells starting from the peak of an immune response.

***Gzma*-FM marks terminal effector CD8$^+$ T cells without memory precursors during the effector phase**. To ensure that *Gzma*-FM signal is turned on specifically during effector CD8$^+$ T cell differentiation, we compared *Gzma*-FM$^+$ vs *Gzma*-FM$^-$ circulating T cells at the effector phase of CD8$^+$ T cell responses. Although *Gzma*-FM signal did not completely overlap with the expression of KLRG1 (**Fig. 3A**), *Gzma*-FM$^+$ subset was enriched for higher KLRG1 and CX3CR1, and lower IL-7R expression (**Fig. 3B**), consistent with the identity of effector T cells. Importantly, *Gzma*-FM$^+$ effector T cells exhibited comparable IFN-g and TNF-a production, and enhanced capacity to produce granzyme B (**Fig. 3C**). Thus, *Gzma*-FM signal is aligned well with an effector CD8$^+$ T cell identity.

When focusing on *Gzma*-FM$^+$ cells, we discovered that current granzyme A-producing cells were poor cytokine producers. Granzyme A protein$^+$ cells exhibited significantly reduced capacity to produce IFN-g and TNF-a, and almost completely abolished IL-2 production (**Fig. 3D** and **3E**). Interestingly, granzyme A protein$^-$ *Gzma*-FM$^+$ cells (ex-granzyme A producers) regained IFN-g and TNF-a producing capacity, even slightly and significantly higher than *Gzma*-FM$^-$ counterparts. IL-2 production was also partially recovered when granzyme A production was terminated (**Fig. 3E**). Importantly, when dividing effector CD8$^+$ T cells based on granzyme B production, we did not observe a significant reduction of IFN-g and TNF-a, while IL-2 was only slightly reduced (**Fig. 3F**). Thus, the expression of granzyme A labels a subset of terminal cytotoxic effector T cells, that transiently lost polyfunctionality.

Tcf-1 (T cell factor-1) is a master transcription factor and well-established marker for memory and memory-precursor T cells[21, 22]. As shown in **Fig. 3G** and **3H**, a Tcf-1$^+$T-bet^{low} subset of memory precursor cells was almost exclusively restricted to the *Gzma*-FM$^-$ subset. When examining the few *Gzma*-FM$^+$ cells that fell into the Tcf-1$^+$ gate, these *Gzma*-FM$^+$ cells carried significantly lower levels of Tcf-1 and CD62L and higher levels of T-bet compared with their *Gzma*-FM$^-$ counterparts (**Fig. 3I**, **3J**, and **3K**). Further, these *Gzma*-FM$^+$ "Tcf-1$^+$" cells were larger in size, suggesting an activated effector, but not a quiescent memory precursor identity (**Fig. 3L**). This evidence strongly supports the conclusion that at the peak of CD8$^+$ effector T cell responses, *Gzma*-FM$^+$ subset is composed of effector T cells, lacking memory precursors. *Gzma*-FM signal is tightly linked to terminal effector CD8$^+$ T cells.

***Gzma*-FM$^+$ effector T cells can dedifferentiate into central memory T cells**. Considering the well-known effector T cell contraction process and the relatively stable frequency of *Gzma*-FM$^+$ T cells (**Fig. 2E**), it raised the possibility that *Gzma*-FM$^+$ terminal effectors can dedifferentiate into memory T cells and survive the contraction phase. To rigorously test this possibility, we examined the CD62L$^+$ T_{CM} and T_{CM} precursors. At the peak of response (day 7-8), CD62L expression was essentially absent in *Gzma*-FM$^+$ cells. As the response progressed into memory phase, we detected a substantial population of CD62L$^+$IL-7Ra$^+$KLRG1$^-$ T_{CM} carrying *Gzma*-FM signal both in spleen and LNs (**Fig. 4A** and **4B**). Although

Gzma-FM$^+$ cells carried less T_{CM} or T_{CM} precursors, the fold of reduction gradually waned. In the spleen, compared with *Gzma*-FM$^-$ counterparts isolated from the same mouse, *Gzma*-FM$^+$ subset carried 9.1±4.1-fold less T_{CM} precursor at day 7 to 8, 7.6±1.7-fold less at day 29 to 35, and 3.0±0.6-fold less at day 61-79 and 1.8±0.5-fold reduction at day 130. In the LNs, the values were 4.3±0.7-fold at day 7-8, 3.6±0.6-fold at day 12-14, 2.3±0.4-fold at day 21-22, 1.17±0.05-fold at day 61 to 79 and 1.04±0.04-fold at day 130 (**Fig. 4A** and **4B**). To estimate the contribution from dedifferentiated terminal effector to memory T cells, we calculated *Gzma*-FM$^+$ cell frequency within the T_{CM} population. There was a steady increase of *Gzma*-FM$^+$ T_{CM} cells in both spleen and LN, reaching around 30% at day 130 post-infection (**Fig. 4C** and **4D**). As shown in **Fig. 4E**, although *Gzma*-FM$^+$CD62L$^-$ cells were enriched for KLRG1$^+$, CX3CR1$^+$, Gzma protein$^+$, CD127^{low} terminal effector memory T cells (t-T_{EM})[23], *Gzma*-FM$^+$CD62L$^+$ cells carried comparable markers as their *Gzma*-FM$^-$ counterparts. Although *Gzma*-FM$^+$ memory population was composed of fewer T_{CM} and more t-T_{EM} (**Fig. 4F**), the expression of Tcf-1 was only slightly reduced in *Gzma*-FM$^+$ T_{CM} around day 70 and completely recovered at day 130 post infection (**Fig. 4G**). For T_{EM} and t-T_{EM}, we detected lower Tcf-1 expression in *Gzma*-FM$^+$ subset (**Fig. 4G**). IL-2 production is a functional feature associated with memory CD8$^+$ T cells, especially T_{CM}. Similar to other T_{CM} markers, there was a steady increase in IL-2 production in *Gzma*-FM$^+$ T cells over time. At day 130 post infection, it was indistinguishable between *Gzma*-FM$^-$ and *Gzma*-FM$^+$ memory T cells in IL-2 production (**Fig. 4G**). In addition to IL-2, *Gzma*-FM$^+$ memory T cells exhibited either comparable or slightly enhanced effector cytokine production compared with *Gzma*-FM$^-$ counterparts (**Fig. S5**). Furthermore, when focusing on polyclonal CD8$^+$ T cells without a TCR transgene, a similar *Gzma*-FM$^+$ T_{CM} subset could be identified (**Fig. S2A** and **S2B**). When enriched memory T cells (*Gzma*-FM$^-$ and *Gzma*-FM$^+$) were subjected to bulk RNA-seq analysis, only subtle differences were detected (**Fig. S4A** and **S4B**). These findings strongly support the conclusion that (1) although with delayed kinetics, *Gzma*-FM$^+$ terminal effector T cells can dedifferentiate into T_{CM}; (2) T_{CM} population is composed of two subsets with distinct differentiation history, i.e., one with a *Gzma*-expressing terminal cytotoxic stage and one without.

***Gzma*-FM$^+$ memory T cells elicit a robust recall response, comparable to *Gzma*-FM$^-$ counterparts**. To further assess the *in vivo* recall responses of dedifferentiated memory T cells, we FACS-sorted *Gzma*-FM$^+$ and *Gzma*-FM$^-$ memory P14 T cells more than 60 days after the primary infection. An equal number of sorted cells were adoptively transferred into naïve secondary recipients, followed by LCMV rechallenge (**Fig. 5A**). When input memory T cells were isolated from d60-80 post-primary infection, *Gzma*-FM$^+$ memory P14 T cells exhibited a slight but significant reduction in recall expansion at day 7. This defect was not due to altered migration because it is consistent across both lymphoid and non-lymphoid tissues (**Fig. 5C** to **5F** top row). At day 13 post recall, the difference in the population size of 2nd effector T cells had largely waned (**Fig. 5C** to **5F** top row). As shown in **Fig. 4**, *Gzma*-FM$^+$ effector T cell dedifferentiation is a slow and progressive process. We repeated this recall experiment using memory P14 T cells isolated from mice that received primary infection 180 days prior. In this setting, we

did not detect any defects in memory T cell recall expansion (**Fig. 5C** to **5F** bottom row). Interestingly, under both settings, we often observed significantly enhanced 2^{nd} effector T cell differentiation, including increased KLRG1, CX3CR1, granzyme A protein, and reduced IL-7R expression in *Gzma*-FM$^+$ memory T cells (**Fig. 5G** to **5J**), suggesting robust imprinting of primary effector differentiation. Together, *Gzma*-FM$^+$ effector-derived memory T cells can gradually regain robust recall capacity and function as long-lived memory T cells.

Discussion

Although it is generally considered redundant for cytotoxic T cells and NK cells, we have demonstrated that the expression of granzyme A, but not granzyme B, tracks the differentiation of terminal effector T cells with skewed cytotoxic capacity and diminished polyfunctionality. Using the *Gzma*-FM system, we discovered that the majority of circulating memory T cells, especially $T_{CM,}$ are derived from early effector T cells without a history of granzyme A expression, supporting the bifurcation model of effector and memory T cell differentiation. Following acute viral infection, granzyme A$^+$ terminal effector T cells do not represent a fixed lineage, but rather a differentiation state. When the level of granzyme A enzyme is reduced, effector CD8$^+$ T cells can rapidly regain the capacity to produce cytokines. *Gzma*-FM$^+$ effector T cells can dedifferentiate into functional T_{CM} cells slowly and progressively, suggesting that the linear differentiation model also contributes to the pool of memory T cells, especially at the late memory stage. Recall response is the defining characteristic of memory T cells. We provided evidence that long-term *Gzma*-FM$^+$ memory T cells exhibit comparable population expansion and distribution during recall response. Interestingly, 2^{nd} effector T cells derived from *Gzma*-FM$^+$ memory T cells are skewed towards KLRG1$^+$ and CX3CR1$^+$ effectors. This finding has two implications. First, the primary response likely leaves epigenetic marks in *Gzma*-FM$^+$ memory T cells, which subsequently steer secondary effector differentiation. Second, *Gzma*-FM$^-$ and *Gzma*-FM$^+$ memory T cells are not completely redundant, but rather play complementary roles during memory recall responses.

As shown in Figure 1, we consistently observe reduced granzyme A expression after TCR stimulation in effector and memory CD8$^+$ T cells. This striking finding can be explained by the fact that granzyme A is pre-made and stored in the mature Golgi apparatus at steady states. Upon TCR stimulation, granzyme A will be rapidly released, the process of which will not be inhibited by commonly available GolgiSTOP or GolgiPlug for intracellular flow cytometry analysis[24]. In contrast, the production of effector cytokines and granzyme B will likely initiate from mRNA translation in memory T cells and require protein export from the endoplasmic reticulum to the Golgi apparatus. Upon Golgi inhibition, cytokines and granzyme B will be accumulated inside the cells.

Previous research has demonstrated that KLRG1$^+$ effector T cells can dedifferentiate into memory T cells[25]. After 30 days post primary infection, exKLRG1 memory T cells exhibited a slight but significant

reduction in recall expansion. Our results show that terminal Gzma^{+} effector T cells undergo a slow dedifferentiation process and gradually regain the recall capacity.

Together, our findings demonstrate that both bifurcation and linear differentiation models are operational during memory T cell differentiation. Memory T cells are composed of a heterogeneous population of cells with distinct differentiation histories. Early bifurcated memory precursors dominate memory T cells immediately after pathogen clearance. A slowly emerging population of dedifferentiated memory T cells gradually joins the pool of circulating memory T cells to provide balanced immune protection.

Materials and Methods

Mice and Virus.

A colony of D^{b}-GP_{33-41} TCR transgenic (P14) mice was maintained in our specific pathogen-free animal facilities at the UT San Antonio Health Science campus (San Antonio, Texas). *Gzma*-Cre mice were generated by the Mouse Genome Engineering and Transgenic Facility at UT Health San Antonio via CRISPR/Cas9-mediated homologous recombination. Briefly, a Cre-T2A-BFP-P2A cassette was inserted before the first exon of *Gzma* gene. Corrected targeting was confirmed by sequencing. Presumably due to dramatically reduced translation efficiency during T2A/P2A-mediated skipping, this is a functional knockout allele without detectable BFP signal (not shown). All experiments were performed using *Gzma*-Cre/+ heterozygous mice. C57BL/6J (B6) (Jax#000664) mice were originally obtained from the Jackson Laboratory. All recipient mice were used at 6 to 10 wk of age. All mice were housed at our specific pathogen-free animal facilities at the University of Texas Health San Antonio. All experiments were conducted in accordance with the National Institutes of Health Guide for the Care and Use of Laboratory Animals and were fully approved by the Institutional Animal Care and Use Committee of the University of Texas Health San Antonio. LCMV Armstrong infection was performed as described before[26]. $2X10^{5}$ pfu LCMV Armstrong was injected into each mouse via an intraperitoneal route.

Staining for Flow Cytometry and Antibodies.

Anti-CD16/32 (2.4G2) was produced in the lab and used in all FACS staining as an FcR blocker. Freshly isolated lymphocytes were stained for surface antigens and incubated for 30 min at 4°C with the following fluorescence dye-labeled antibodies specific for CD8β (H35-17.2), CD45.1 (A20), CD45.2 (104), CD8a (53-6.7), CX3CR1 (SA011F11), CD62L(MEL-14), CD69 (H1.2F3), CD127 (A7R34), KLRG1 (2F1/KLRG1) were purchased from Thermo Fisher, Biolegend, and Cytek (Cytek/Tonbo). For live cell staining, Ghost Dye Violet 510 (Cytek/Tonbo) was used. For intranuclear staining, cells were fixed following surface staining and permeabilized with the FOXP3/Transcription Factor staining buffer kit (Cytek/Tonbo) for 45 min at room temperature and then stained with anti-Tcf-1 (C63D9, Cell Signaling) and anti-T-bet (4B10, Invitrogen). For intracellular cytokine staining, freshly isolated lymphocytes were cultured with or without 1mM GP_{33-41} peptide (AnaSpec) in the presence of Golgi Stop^{TM} (BD) for 4-5 hours at 37°C. After surface staining, fixation and permeabilization using permeabilization buffer

(Invitrogen), the following antibodies IL-2 (JES6-5H4), TNFa (MP6-XT22), IFNg (XMG1.2), Granzyme A (3G8.5), and Granzyme B (GB11) were incubated with the samples at 4°C for 30 min. Washed and fixed samples were collected by BD FACSCelesta, BD FACSymphony A5, and analyzed by FlowJo (TreeStar) software.

Naïve T Cell Isolation, Adoptive Transfer and Memory Recall Response.

Naïve $CD8^+$ T cells were isolated from pooled spleen and lymph nodes using MojoSort™ mouse CD8 T cell isolation kit (Biolegend) following the manufacturer's instructions. Following enrichment, $CD44^{low}tdTomato^-$ naïve $CD8^+$ T cells were FACS sorted using a BD Aria Fusion. $5x10^3$-$1x10^4$ sorted cells were adoptively transferred into each sex-matched unmanipulated B6 recipient via an i.v. route followed by LCMV Arm infection.

At indicated times post-infection, lymphocytes were isolated from pooled spleen and LNs. Following $CD8^+$ T cell magnetic enrichment, $CD8^+CD45.1^+tdTomato^+$ and $CD8^+CD45.1^+$ $tdTomato^-$ memory T cells were FACS sorted using a BD Aria Fusion. 5,000 to 7,000 sorted memory T cells were adoptively transferred into each sex-matched naïve B6 recipient via an i.v. route followed by LCMV Arm infection.

Lymphocyte Isolation from Non-lymphoid Tissues.

Small intestine: Lymphocyte isolation procedures have been described before[26]. Briefly, small pieces of the small intestine were stirred at 800 rpm for 20 min in HBSS buffer containing 1mM dithiothreitol and 10% FCS at 37°C to release IEL. The remaining pieces of small intestine were further digested by 0.08U/ml Liberase TL (Sigma, 5401020001) + 200U/ml DNase I (Sigma, D5025) + 1.33mg/ml Dispase II (Sigma, D4693) with stirring for 45 min at 37°C. Both digested LP and released IEL were further purified by density gradient centrifugation with PBS-balanced 44% and 67% Percoll (GE Healthcare). Lymphocyte isolation from other non-lymphoid tissues has been described before[27, 28]. Briefly, kidney, liver, and SG was minced and digested with 1mg/ml collagenase B (Roche) in RPMI 1640/3% FCS at 37°C for 30-45 mins with gentle shaking. Digested tissues were further mashed and washed with RPMI 1640/10% FCS. Digested tissues were further purified by gradient centrifugation with PBS-balanced 44% and 67% Percoll (GE Healthcare).

Immediate Memory Recall by Cognate Peptide or Bystander Inflammation.

After 30 days of LCMV infection, we re-challenged one group of mice with $2x10^5$ cfu/mouse LM via an i.v. route. On the following day, 250mg Brefeldin A (B6542, Sigma) in 200ml PBS was injected i.v. 4 hours before euthanasia, similar to a previous report[29]. One group of mice received 32mg/mouse GP_{33-41} peptide i.v. (Genscript) together with Brefeldin A. During the lymphocyte isolation procedure, 5mg/ml Brefeldin A was added. Freshly isolated lymphocytes were surface-stained, fixed, permeabilized, and intracellularly stained.

Intra-vascular Labeling of $CD8^+$ T Cells.

3mg biotin-aCD8a (53-6.7, Tonbo Biosciences) was injected i.v. 5 mins before euthanasia. After lymphocyte isolation, fluorescence-labeled streptavidin (Thermo Fisher) was used during surface staining to identify blood-borne $CD8^+$ T cells.

RNA-seq Analysis.

Indicated P14 T cell subsets were FACS sorted, and RNA was extracted from sorted cells using the Quick-RNA MiniPrep according to the manufacturer's instructions (Zymo Research). RNA-seq analysis was performed by Novogene.

Statistical Analysis.

P value was calculated by two-tail paired or unpaired Student *t*-test, One-way ANOVA using Prism 10 software.

Declarations

Acknowledgement.

We thank Drs. Susan Kaech and Barbara Kee for the helpful discussion about *Gzmb*-FM mice. H2-D^b-GP_{33-41} tetramer was obtained through the NIH Tetramer Core Facility. We thank Dr. Yue Li, Catherine Davis, and Anastassia Nelson for FACS sorting. Data generated in the Flow Cytometry Shared Resource Facility, which is supported by a grant from the National Cancer Institute (P30CA054174) to the Mays Cancer Center, a grant from the Cancer Prevention and Research Institute of Texas (CPRIT) (RP210126), a grant from the National Institutes of Health (S10OD030432), and support from the Office of the Vice President for Research at UT Health San Antonio.

Data Availability Statement.

RNA-seq results can be accessed by GSE336218. Other data are available from the corresponding authors upon reasonable request.

References

1. Kaech SM, Cui W. Transcriptional control of effector and memory CD8 + T cell differentiation. Nat Rev Immunol. 2012;12(11):749–61. Epub 20121019. doi: 10.1038/nri3307. PubMed PMID: 23080391; PMCID: PMC4137483.
2. Akondy RS, Fitch M, Edupuganti S, Yang S, Kissick HT, Li KW, Youngblood BA, Abdelsamed HA, McGuire DJ, Cohen KW, Alexe G, Nagar S, McCausland MM, Gupta S, Tata P, Haining WN, McElrath MJ, Zhang D, Hu B, Greenleaf WJ, Goronzy JJ, Mulligan MJ, Hellerstein M, Ahmed R. Origin and

differentiation of human memory CD8 T cells after vaccination. Nature. 2017;552(7685):362–7. Epub 20171213. doi: 10.1038/nature24633. PubMed PMID: 29236685; PMCID: PMC6037316.

3. Youngblood B, Hale JS, Kissick HT, Ahn E, Xu X, Wieland A, Araki K, West EE, Ghoneim HE, Fan Y, Dogra P, Davis CW, Konieczny BT, Antia R, Cheng X, Ahmed R. Effector CD8 T cells dedifferentiate into long-lived memory cells. Nature. 2017;552(7685):404–9. Epub 20171213. doi: 10.1038/nature25144. PubMed PMID: 29236683; PMCID: PMC5965677.
4. Bannard O, Kraman M, Fearon DT. Secondary replicative function of CD8 + T cells that had developed an effector phenotype. Science. 2009;323(5913):505–9. doi: 10.1126/science.1166831. PubMed PMID: 19164749; PMCID: PMC2653633.
5. Jacob J, Baltimore D. Modelling T-cell memory by genetic marking of memory T cells in vivo. Nature. 1999;399(6736):593–7. doi:
10.
1038/21208. PubMed PMID: 10376601.
6. Opferman JT, Ober BT, Ashton-Rickardt PG. Linear differentiation of cytotoxic effectors into memory T lymphocytes. Science. 1999;283(5408):1745–8. doi: 10.1126/science.283.5408.1745. PubMed PMID: 10073942.
7. Lucas ED, Huggins MA, Peng C, O'Connor C, Gress AR, Thefaine CE, Dehm EM, Kubota Y, Jameson SC, Hamilton SE. Circulating KLRG1(+) long-lived effector memory T cells retain the flexibility to become tissue resident. Sci Immunol. 2024;9(96):eadj8356. Epub 20240628. doi: 10.1126/sciimmunol.adj8356. PubMed PMID: 38941479; PMCID: PMC12175144.
8. Pais Ferreira D, Silva JG, Wyss T, Fuertes Marraco SA, Scarpellino L, Charmoy M, Maas R, Siddiqui I, Tang L, Joyce JA, Delorenzi M, Luther SA, Speiser DE, Held W. Central memory CD8(+) T cells derive from stem-like Tcf7(hi) effector cells in the absence of cytotoxic differentiation. Immunity. 2020;53(5):985–1000 e11. Epub 20201030. doi: 10.1016/j.immuni.2020.09.005. PubMed PMID: 33128876.
9. Chang JT, Palanivel VR, Kinjyo I, Schambach F, Intlekofer AM, Banerjee A, Longworth SA, Vinup KE, Mrass P, Oliaro J, Killeen N, Orange JS, Russell SM, Weninger W, Reiner SL. Asymmetric T lymphocyte division in the initiation of adaptive immune responses. Science. 2007;315(5819):1687–91. Epub 20070301. doi: 10.1126/science.1139393. PubMed PMID: 17332376.
10. Restifo NP, Gattinoni L. Lineage relationship of effector and memory T cells. Curr Opin Immunol. 2013;25(5):556–63. Epub 20131020. doi: 10.1016/j.coi.2013.09.003. PubMed PMID: 24148236; PMCID: PMC3858177.
11. Johnnidis JB, Muroyama Y, Ngiow SF, Chen Z, Manne S, Cai Z, Song S, Platt JM, Schenkel JM, Abdel-Hakeem M, Beltra JC, Greenplate AR, Ali MA, Nzingha K, Giles JR, Harly C, Attanasio J, Pauken KE, Bengsch B, Paley MA, Tomov VT, Kurachi M, Vignali DAA, Sharpe AH, Reiner SL, Bhandoola A, Johnson FB, Wherry EJ. Inhibitory signaling sustains a distinct early memory CD8(+) T cell precursor that is resistant to DNA damage. Sci Immunol. 2021;6(55). doi: 10.1126/sciimmunol.abe3702. PubMed PMID: 33452106; PMCID: PMC8258400.

12. Kretschmer L, Flossdorf M, Mir J, Cho YL, Plambeck M, Treise I, Toska A, Heinzel S, Schiemann M, Busch DH, Buchholz VR. Differential expansion of T central memory precursor and effector subsets is regulated by division speed. Nat Commun. 2020;11(1):113. Epub 20200108. doi: 10.1038/s41467-019-13788-w. PubMed PMID: 31913278; PMCID: PMC6949285.
13. Lin WW, Nish SA, Yen B, Chen YH, Adams WC, Kratchmarov R, Rothman NJ, Bhandoola A, Xue HH, Reiner SL. CD8(+) T Lymphocyte Self-Renewal during Effector Cell Determination. Cell Rep. 2016;17(7):1773–82. doi: 10.1016/j.celrep.2016.10.032. PubMed PMID: 27829149; PMCID: PMC5108530.
14. Plambeck M, Kazeroonian A, Loeffler D, Kretschmer L, Salinno C, Schroeder T, Busch DH, Flossdorf M, Buchholz VR. Heritable changes in division speed accompany the diversification of single T cell fate. Proc Natl Acad Sci U S A. 2022;119(9). doi: 10.1073/pnas.2116260119. PubMed PMID: 35217611; PMCID: PMC8892279.
15. Scherer S, Oberle SG, Kanev K, Gerullis AK, Wu M, de Almeida GP, Puleston DJ, Baixauli F, Aly L, Greco A, Nizharadze T, Becker NB, Hoesslin MV, Donhauser LV, Berner J, Chu T, McNamara HA, Esencan Z, Roelli P, Wurmser C, Kleiter I, Vehreschild M, Mayer CA, Knolle P, Klingenspor M, Fumagalli V, Iannacone M, Prlic M, Korn T, Pearce EL, Hofer T, Schulz AM, Zehn D. Pyrimidine de novo synthesis inhibition selectively blocks effector but not memory T cell development. Nat Immunol. 2023;24(3):501–15. Epub 20230216. doi: 10.1038/s41590-023-01436-x. PubMed PMID: 36797499.
16. Hale BD, Severin Y, Graebnitz F, Stark D, Guignard D, Mena J, Festl Y, Lee S, Hanimann J, Zangger NS, Meier M, Goslings D, Lamprecht O, Frey BM, Oxenius A, Snijder B. Cellular architecture shapes the naive T cell response. Science. 2024;384(6700):eadh8697. Epub 20240607. doi: 10.1126/science.adh8967. PubMed PMID: 38843327.
17. Guo A, Huang H, Zhu Z, Chen MJ, Shi H, Yuan S, Sharma P, Connelly JP, Liedmann S, Dhungana Y, Li Z, Haydar D, Yang M, Beere H, Yustein JT, DeRenzo C, Pruett-Miller SM, Crawford JC, Krenciute G, Roberts CWM, Chi H, Green DR. cBAF complex components and MYC cooperate early in CD8(+) T cell fate. Nature. 2022;607(7917):135–41. Epub 20220622. doi: 10.1038/s41586-022-04849-0. PubMed PMID: 35732731; PMCID: PMC9623036.
18. Nizharadze T, Becker NB, Hofer T. Quantitating CD8(+) T cell memory development. Trends Immunol. 2023;44(7):519–29. Epub 20230604. doi: 10.1016/j.it.2023.05.004. PubMed PMID: 37277233.
19. Liu Z, Chen O, Wall JBJ, Zheng M, Zhou Y, Wang L, Vaseghi HR, Qian L, Liu J. Systematic comparison of 2A peptides for cloning multi-genes in a polycistronic vector. Sci Rep. 2017;7(1):2193. Epub 20170519. doi: 10.1038/s41598-017-02460-2. PubMed PMID: 28526819; PMCID: PMC5438344.
20. Kernfeld EM, Genga RMJ, Neherin K, Magaletta ME, Xu P, Maehr R. A Single-Cell Transcriptomic Atlas of Thymus Organogenesis Resolves Cell Types and Developmental Maturation. Immunity. 2018;48(6):1258–70 e6. Epub 20180605. doi: 10.1016/j.immuni.2018.04.015. PubMed PMID: 29884461; PMCID: PMC6013397.
21. Gounari F, Khazaie K. TCF-1: a maverick in T cell development and function. Nat Immunol. 2022;23(5):671–8. Epub 20220429. doi: 10.1038/s41590-022-01194-2. PubMed PMID: 35487986;

PMCID: PMC9202512.

22. Zhao X, Shan Q, Xue HH. TCF1 in T cell immunity: a broadened frontier. Nat Rev Immunol. 2022;22(3):147–57. Epub 20210614. doi: 10.1038/s41577-021-00563-6. PubMed PMID: 34127847.
23. Milner JJ, Nguyen H, Omilusik K, Reina-Campos M, Tsai M, Toma C, Delpoux A, Boland BS, Hedrick SM, Chang JT, Goldrath AW. Delineation of a molecularly distinct terminally differentiated memory CD8 T cell population. Proc Natl Acad Sci U S A. 2020;117(41):25667–78. Epub 20200925. doi: 10.1073/pnas.2008571117. PubMed PMID: 32978300; PMCID: PMC7568335.
24. Hendricks LC, McClanahan SL, Palade GE, Farquhar MG. Brefeldin A affects early events but does not affect late events along the exocytic pathway in pancreatic acinar cells. Proc Natl Acad Sci U S A. 1992;89(15):7242–6. doi: 10.1073/pnas.89.15.7242. PubMed PMID: 1496018; PMCID: PMC49682.
25. Herndler-Brandstetter D, Ishigame H, Shinnakasu R, Plajer V, Stecher C, Zhao J, Lietzenmayer M, Kroehling L, Takumi A, Kometani K, Inoue T, Kluger Y, Kaech SM, Kurosaki T, Okada T, Flavell RA. KLRG1(+) Effector CD8(+) T Cells Lose KLRG1, Differentiate into All Memory T Cell Lineages, and Convey Enhanced Protective Immunity. Immunity. 2018;48(4):716–29 e8. Epub 20180403. doi: 10.1016/j.immuni.2018.03.015. PubMed PMID: 29625895; PMCID: PMC6465538.
26. Wang L, Mishra S, Fan KK, Quon S, Li G, Yu B, Liao W, Liu Y, Zhang X, Qiu Y, Li Y, Goldrath AW, Ma C, Zhang N. T-bet deficiency and Hic1 induction override TGF-beta-dependency in the formation of CD103(+) intestine-resident memory CD8(+) T cells. Cell Rep. 2024;43(6):114258. Epub 20240522. doi: 10.1016/j.celrep.2024.114258. PubMed PMID: 38781073; PMCID: PMC11240284.
27. Ma C, Mishra S, Demel EL, Liu Y, Zhang N. TGF-beta Controls the Formation of Kidney-Resident T Cells via Promoting Effector T Cell Extravasation. J Immunol. 2017;198(2):749–56. Epub 20161130. doi: 10.4049/jimmunol.1601500. PubMed PMID: 27903738; PMCID: PMC5225110.
28. Zhang N, Bevan MJ. Transforming growth factor-beta signaling controls the formation and maintenance of gut-resident memory T cells by regulating migration and retention. Immunity. 2013;39(4):687–96. doi: 10.1016/j.immuni.2013.08.019. PubMed PMID: 24076049; PMCID: PMC3805703.
29. Kovacs SB, Oh C, Aachoui Y, Miao EA. Evaluating cytokine production by flow cytometry using brefeldin A in mice. STAR Protoc. 2021;2(1):100244. Epub 20201230. doi: 10.1016/j.xpro.2020.100244. PubMed PMID: 33458706; PMCID: PMC7797915.

Figures

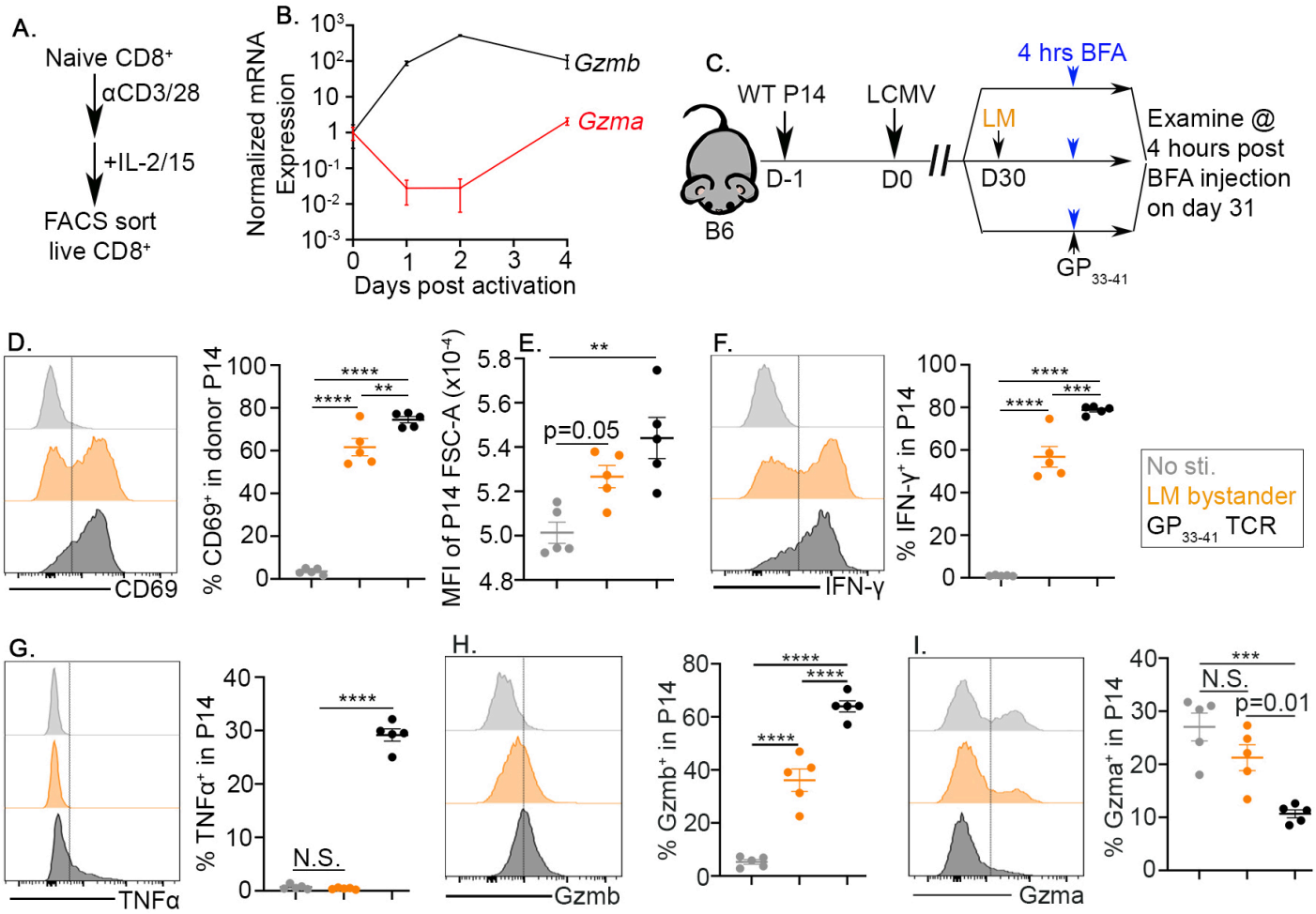


Figure 1

Distinct expression patterns of granzyme A and granzyme B. (**A**) Experimental setup for (B). (**B**) mRNA levels for *Gzma* and *Gzmb* during naïve CD8$^+$ T cell activation *in vitro*. (**C**) Experimental setup for (D) to (I). Pre-gated on splenic P14 T cells, (**D**) the expression of CD69, (**E**) mean fluorescence intensity (MFI) of FSC-A, (**F**) IFN-g, (**G**) TNF-a, (**H**) granzyme B, and (**I**) granzyme A production are shown. Each symbol represents the results from an individual mouse. **, p<0.01, ***, p<0.001 and ****, p<0.0001 by one-way ANOVA. Representative results from two independent repeats are shown.

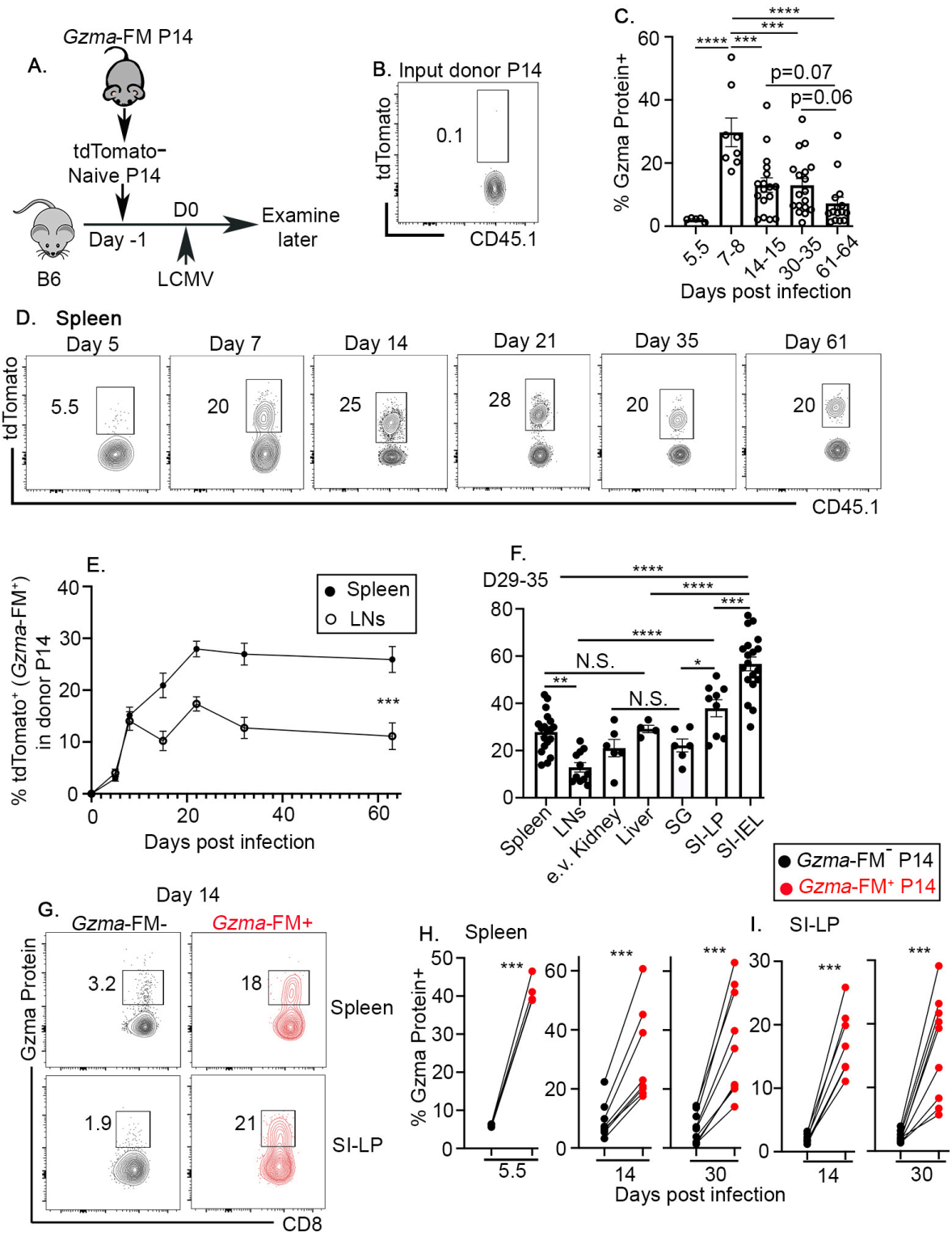


Figure 2

***Gzma*-FM tracks a subset of effector and memory CD8$^+$ T cells**. (**A**) Experimental setup. (**B**) Representative FACS profile to show input *Gzma*-FM$^-$ P14 T cells. (**C**) The percentage of Gzma protein$^+$ cells in donor P14 T cells isolated from the spleen is shown. (**D**) Representative FACS profiles of pre-gated donor P14 T cells isolated from the spleen. (**E**) and (**F**), the percentage of *Gzma*-FM$^+$ cells within donor P14 T cells isolated from indicated tissues. Mean±SEM (n=10-20/time point) is shown in (E). (**G**)

Representative FACS profiles of pre-gated *Gzma*-FM$^-$ (left) and *Gzma*-FM$^+$ (right) donor P14 T cells are shown. The percentage of Gzma protein$^+$ cells within indicated subsets of donor P14 T cells isolated from (**H**) spleen and (**I**) small intestine lamina propria (SI-LP) is shown. Each symbol in (C and F) and each pair of symbols in (H and I) represents the results from an individual recipient mouse. *, p<0.05, **, p<0.01, ***, p<0.001 and ****, p<0.0001 by one-way ANOVA (C and F) or paired Student *t*-test (H, I). Pooled results from 4-5 independent experiments are shown.

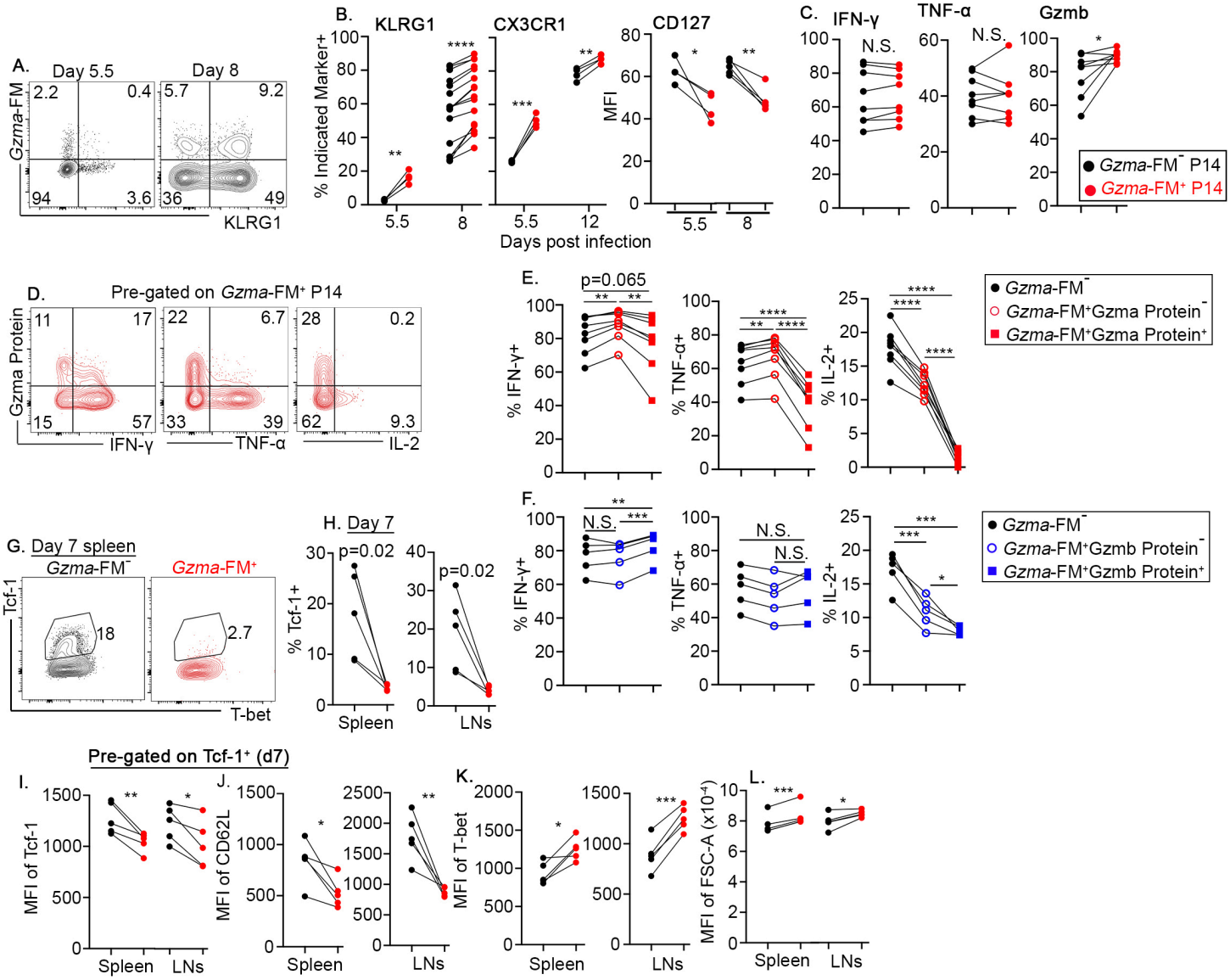


Figure 3

***Gzma*-FM tracks terminal effector T cell differentiation**. Similar setup as in Fig. 2A. (**A**) Representative FACS profiles of pre-gated donor P14 T cells isolated from the spleen are shown. (**B**) The frequency of KLRG1$^+$ (left) and CX3CR1$^+$ (middle) cells, and the MFI of CD127 (right) within *Gzma*-FM$^-$ and *Gzma*-FM$^+$ P14 T cells are shown. (**C**) After *ex vivo* stimulation, the frequency of IFN-g$^+$ (left), TNF-a$^+$ (middle), and granzyme B$^+$ (right) is shown. (**D**) Representative FACS profiles of pre-gated *Gzma*-FM$^+$ P14 T cells (d14

spleen) are shown. (**E**) The production of IFN-g (left), TNF-a (middle), and IL-2 (right) by *Gzma*-FM$^-$ (black dot), *Gzma*-FM$^+$ Gzma protein$^-$ (red circle), and *Gzma*-FM$^+$ Gzma protein$^+$ (red square) cells is shown. (**F**) The production of IFN-g (left), TNF-a (middle), and IL-2 (right) by *Gzma*-FM$^-$ (black dot), *Gzma*-FM$^+$ Gzmb protein$^-$ (blue circle), and *Gzma*-FM$^+$ Gzmb protein$^+$ (blue square) cells is shown. Day 7 post-infection, (**G**) Representative FACS profiles of pre-gated *Gzma*-FM$^-$ (left) and *Gzma*-FM$^+$ (right) P14 T cells isolated from the spleen are shown. (**H**) The percentage of Tcf-1$^+$ cells in *Gzma*-FM$^-$ and *Gzma*-FM$^+$ subsets is shown. Pre-gated on Tcf-1$^+$ cells, (**I**) MFI of Tcf-1, (**J**) CD62L, (**K**) T-bet, and (**J**) FSC-A are shown. Each connected group of symbols represents the results from one mouse. Pooled results from 2 to 5 independent repeats are shown. N.S., not significant, *, p<0.05, **, p<0.01, ***, p<0.001 and ****, p<0.0001 by paired Student *t*-test.

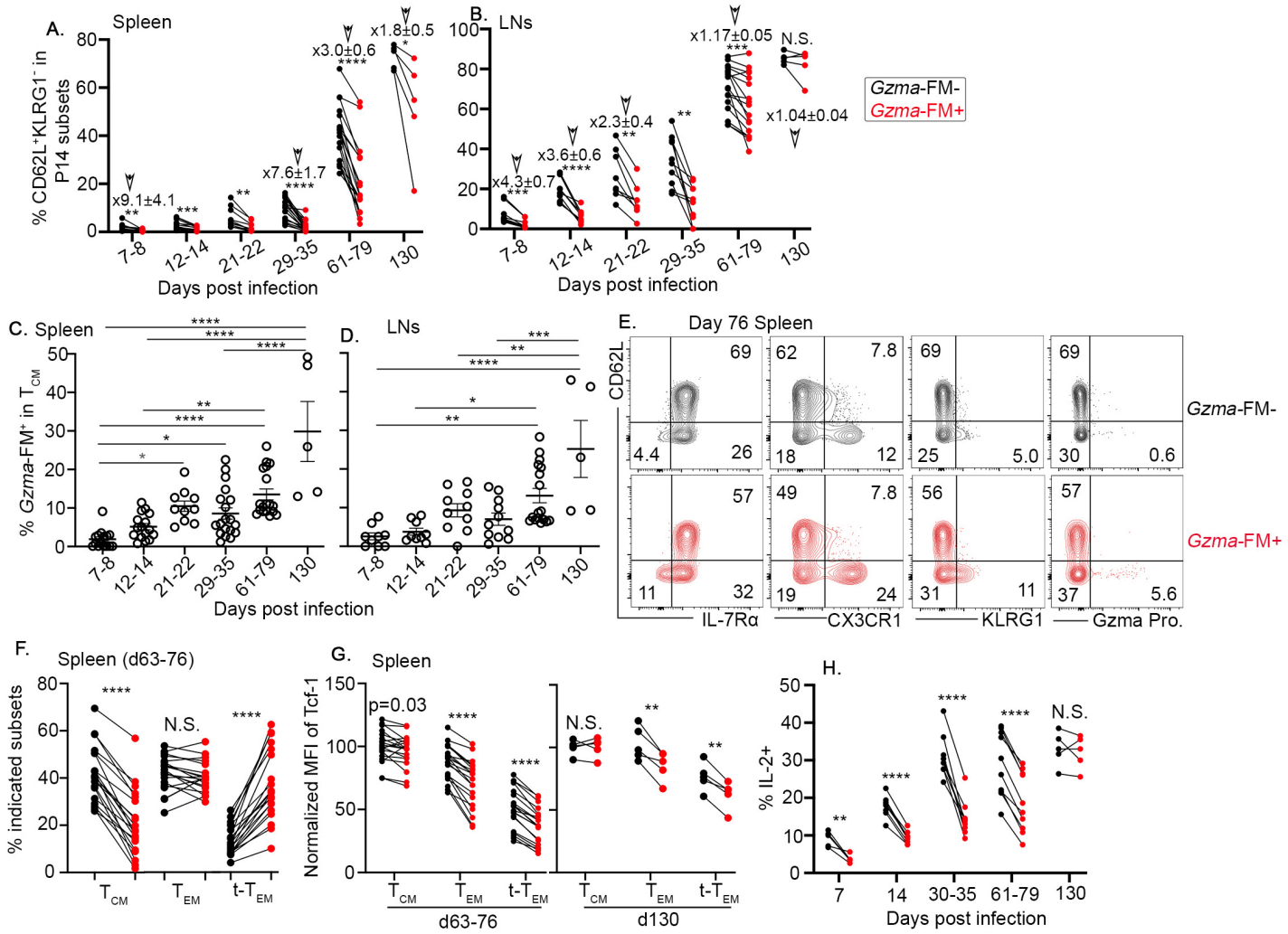


Figure 4

***Gzma*-FM$^+$ effector T cells progressively dedifferentiate into T_{CM}.** Similar setup as in Fig. 2A. At the indicated times post-infection, the percentage of CD62L$^+$KLRG1$^-$ cells within *Gzma*-FM$^-$ and *Gzma*-FM$^+$ P14 subsets isolated from the spleen (**A**) and LNs (**B**) is shown. Within pre-gated CD62L$^+$KLRG1$^-$ P14 T

cells isolated from the spleen (**C**) and LNs (**D**), the percentage of *Gzma*-FM^{+} cells is shown. (**E**) Representative flow cytometry profiles of pre-gated *Gzma*-FM^{-} (upper) and *Gzma*-FM^{+} (lower) P14 memory T cells. (**F**) The percentage of T_{CM} (left), T_{EM} (middle, CD62L^{-}CD127^{+}) and t-T_{EM} (right, CD62L^{-} CD127^{-}) among *Gzma*-FM^{-} and *Gzma*-FM^{+} memory P14 T cells is shown. (**G**) MFI of Tcf-1 in *Gzma*-FM^{-} and *Gzma*-FM^{+} T_{CM}, $T_{EM,}$ and t-T_{EM} P14 T cells is shown. (**H**) IL-2 production from *Gzma*-FM^{-} and *Gzma*-FM^{+} P14 T cells after *ex vivo* stimulation is shown. Each pair of connected symbols in (A), (B), (F), (G), and (H), and each symbol in (C) and (D) represents the results from one mouse. Pooled results from 4-5 independent repeats. N.S., not significant, *, p<0.05, **, p<0.01, ***, p<0.001, and ****, p<0.0001 by paired Student *t*-test (A, B, F, G, H) or one-way ANOVA (C, D).

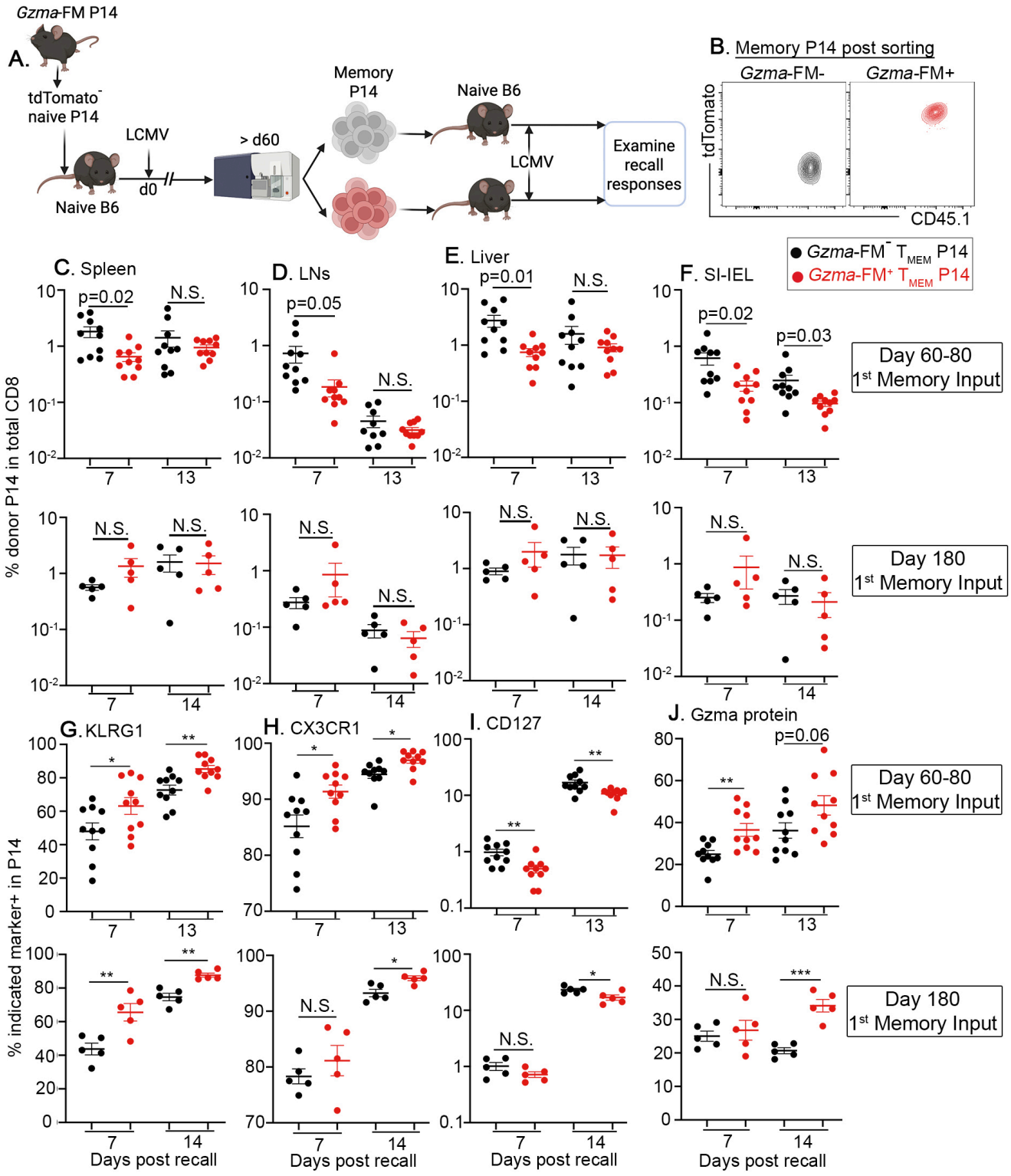


Figure 5

Comparable recall responses of long-lived *Gzma*-FM$^+$ memory T cells. (**A**) Experimental design. (**B**) Representative FACS profiles of sorted *Gzma*-FM$^-$ and *Gzma*-FM$^+$ memory P14 T cells before secondary transfer are shown. At indicated times (d7 or d13-14) post recall, the percentage of donor P14 T cells in total CD8$^+$ T cells in (**C**) Spleen, (**D**) LNs, (**E**) Liver, and (**F**) SI-IEL of secondary recipients is shown. The

expression of (**G**) KLRG1, (**H**) CX3CR1, (**I**) CD127, and (**J**) Gzma protein in 2nd effector T cells isolated from the spleen is shown. Input memory T cells were sorted from day 60-80 (upper row) and day 180 (lower row) post-primary infection. Each symbol represents an individual 2nd recipient mouse. Pooled results from 3 independent repeats are shown. N.S., not significant, *, p<0.05, **, p<0.01, ***, p<0.001 and ****, p<0.0001 by Student *t*-test.

Supplementary Files

This is a list of supplementary files associated with this preprint. Click to download.

- SupplementalFiguresupdated.docx